Surface-induced piezomagnetic, piezoelectric, and linear magnetoelectric effects in nanosystems

E. A. Eliseev,[1,*] A. N. Morozovska,[2] M. D. Glinchuk,[1] B. Y. Zaulychny,[1] V. V. Skorokhod,[1] and R. Blinc[3]

[1]*Institute for Problems of Materials Science, National Academy of Sciences of Ukraine, Krjijanovskogo 3, 03142 Kiev, Ukraine*
[2]*V. Lashkarev Institute of Semiconductor Physics, National Academy of Sciences of Ukraine, prospect Nauki 41, 03028 Kiev, Ukraine*
[3]*Jožef Stefan Institute, P.O. Box 3000, 1001 Ljubljana, Slovenia*

Using symmetry theory we explore how symmetry breaking inevitably present in the vicinity of any surface gives rise to spontaneous surface piezomagnetic, piezoelectric, and magnetoelectric effects. The large surface-to-volume ratio makes the surface symmetry effects dominant in small enough nanosystems. As a result piezomagnetism, piezoelectricity, and strong size-dependent linear magnetoelectric coupling are predicted in nanomaterials, which are nonpiezomagnetic and/or nonpiezoelectric in the bulk, but belong to the one of the existing 90 bulk magnetic classes, e.g., among a wide class of cubic binary oxides such as MnO, FeO, CoO, NiO, EuO, PrO, and Er_2O_3.

I. INTRODUCTION

Symmetry breaking present in the vicinity of any surface is the source of intriguing modifications of the interface structure, their polar and magnetic states.[1–4] Recent atomistic calculations should be considered as the manifestation of strong Dzyaloshinskii-Moriya (DM) interaction in nanosystems.[1–4] Actually, the symmetry lowering near the surface could strongly increase the symmetry related Dzyaloshinskii-Moriya vector value and change its direction.[4] Based on these results one can expect weak ferromagnetism in different nanosystems while the corresponding bulk material may be antiferromagnetic.

Actually, Bode *et al.*[1] revealed experimentally the spiral magnetic order with a period of about 12 nm in a single atomic layer of manganese on a tungsten (110) substrate. Using the spin-polarized scanning tunneling microscopy, they observed that adjacent spins are not perfectly antiferromagnetic but slightly canted, resulting in a spin spiral structure. Using the density-functional theory, Bode *et al.*[1] proved that the spin order is caused by the DM interaction, which arises from spin-orbit scattering of electrons in an inversion-asymmetric crystal field. Raedt *et al.*[2] theoretically studied effects of the DM interaction on the adiabatic magnetization dynamics in molecular nanomagnets V_{15} and Mn_{12}. They show that DM interaction is the most plausible source for the energy-level repulsions that leads to adiabatic changes in the magnetization. On the basis of first-principles calculations in combination with a micromagnetic model Heide *et al.*[3] have shown that for a two monolayers thick Fe film on W(110) the DM interaction determines the orientation of magnetic domains relative to the lattice, the type of domain wall, and the rotational direction of the magnetization in the wall. Using first-principles calculations and Green's-function formalism Rudenko *et al.*[4] investigated electronic and magnetic structures of the Mn antiferromagnetic chains supported on the CuN surface. They predict a weak ferromagnetism in the nanochains caused by surface-enhanced DM interactions and expect the weak ferromagnetism phenomenon in the similar surface nanosystems. The main source of this phenomenon is local distortion that breaks the inversion symmetry between Mn atoms.

Symmetry breaking is especially important in small enough nanosystems, where the surface symmetry effect may become dominant for the whole system because of the large surface-to-volume ratio, leading to new properties absent in bulk.[5–10] For example, such striking phenomena as the observation of ferromagnetism in spherical nanoparticles (size 7–30 nm) of nonmagnetic oxides CeO_2, Al_2O_3, ZnO, etc., have been reported.[5] Strong superparamagnetic behavior down to 4 K has been found in gold and palladium nanoparticles with mean diameter 2.5 nm and a narrow size distribution.[6] Ferroelectric phase transition appears in thin antiferroelectric $PbZrO_3$ and $BiNbO_4$ films when their thickness decreases.[7] A strong enhancement of the spontaneous polarization and a persistence of the ferroelectric phase up to the chemical decomposition have been observed in Rochelle salt nanorods of diameter 30 nm.[8] The appearance of ferroelectricity takes place in nanosized incipient ferroelectrics, which remain paraelectric up to 0 K in the bulk.[9,11] Er_2O_3 that is paramagnetic and paraelectric in the bulk becomes ferroelectric and strongly magnetoelectric (ME) at room temperature if it is put in the form of 5–6 nm size nanoparticles in an insulating matrix.[12]

All these various facts (which are only a small subjective selection from the available great number) illustrate how extremely important surface influence can be the on the electronic, polar, and magnetic properties as well as their coupling for nanomaterials. Despite the great importance for nanoscience, the unified theory of the surface-induced phenomena is currently absent. Thus a theoretical approach capable to study different polar and magnetic properties and especially to predict new effects and couplings in nanosystems seems rather important for both fundamental science and useful for the design of new functional nanomaterials with prominent applications. In particular, the ME effect, i.e., induction of magnetization by an electric field or of polarization by a magnetic field, attracted broad interest in the recent years,[13–16] while the features of ME coupling remains virtually unexplored in nanosystems. The vital interest to the piezoelectric (PE) and piezomagnetic (PM) effects in nanomaterials is determined by their multiple novel applications.[14,17]

While the existence of the PE effect in the vicinity of surface was shown earlier,[18] the supposition about the ap-

TABLE I. Surface and bulk PE, PM, and ME tensors in Voigt notation.

Symmetry group	Piezomagnetic tensor	Piezoelectric tensor	Linear ME tensor
Bulk $m3m$, $m'3m$	Absent in the bulk $d_{ijk}^{(m)} \equiv 0$	Absent in the bulk $d_{ijk}^{(e)} \equiv 0$	Absent $\gamma_{ij} = 0$
Bulk $m'3m'$	Absent in the bulk $d_{ijk}^{(m)} \equiv 0$	Absent in the bulk $d_{ijk}^{(e)} \equiv 0$	$\begin{pmatrix} \gamma_{11} & 0 & 0 \\ 0 & \gamma_{11} & 0 \\ 0 & 0 & \gamma_{11} \end{pmatrix}$
Bulk $m3m'$	$\begin{pmatrix} 0 & 0 & 0 & d_{14}^{(m)} & 0 & 0 \\ 0 & 0 & 0 & 0 & d_{14}^{(m)} & 0 \\ 0 & 0 & 0 & 0 & 0 & d_{14}^{(m)} \end{pmatrix}$	Absent in the bulk $d_{ijk}^{(e)} \equiv 0$	Absent $\gamma_{ij} = 0$
Surface $4mm$	$\begin{pmatrix} 0 & 0 & 0 & d_{14}^{(Sm)} & 0 & 0 \\ 0 & 0 & 0 & 0 & -d_{14}^{(Sm)} & 0 \\ 0 & 0 & 0 & 0 & 0 & 0 \end{pmatrix}$	$\begin{pmatrix} 0 & 0 & 0 & 0 & d_{15}^{(Se)} & 0 \\ 0 & 0 & 0 & d_{15}^{(Se)} & 0 & 0 \\ d_{31}^{(Se)} & d_{31}^{(Se)} & d_{33}^{(Se)} & 0 & 0 & 0 \end{pmatrix}$	$\begin{pmatrix} 0 & \gamma_{12}^{S} & 0 \\ -\gamma_{12}^{S} & 0 & 0 \\ 0 & 0 & 0 \end{pmatrix}$
Surface $4m'm'$	$\begin{pmatrix} 0 & 0 & 0 & 0 & d_{15}^{(Sm)} & 0 \\ 0 & 0 & 0 & d_{15}^{(Sm)} & 0 & 0 \\ d_{31}^{(Sm)} & d_{31}^{(Sm)} & d_{33}^{(Sm)} & 0 & 0 & 0 \end{pmatrix}$	The same as above	$\begin{pmatrix} \gamma_{11}^{S} & 0 & 0 \\ 0 & \gamma_{11}^{S} & 0 \\ 0 & 0 & \gamma_{33}^{S} \end{pmatrix}$
Surface $4'mm'$[a]	$\begin{pmatrix} 0 & 0 & 0 & d_{14}^{(Sm)} & 0 & 0 \\ 0 & 0 & 0 & 0 & d_{14}^{(Sm)} & 0 \\ 0 & 0 & 0 & 0 & 0 & d_{36}^{(Sm)} \end{pmatrix}$	The same as above	$\begin{pmatrix} 0 & \gamma_{12}^{S} & 0 \\ \gamma_{12}^{S} & 0 & 0 \\ 0 & 0 & 0 \end{pmatrix}$
Surface $4'm'm$[a]	$\begin{pmatrix} 0 & 0 & 0 & 0 & d_{15}^{(Sm)} & 0 \\ 0 & 0 & 0 & -d_{15}^{(Sm)} & 0 & 0 \\ d_{31}^{(Sm)} & -d_{31}^{(Sm)} & 0 & 0 & 0 & 0 \end{pmatrix}$	The same as above	$\begin{pmatrix} \gamma_{11}^{S} & 0 & 0 \\ 0 & -\gamma_{11}^{S} & 0 \\ 0 & 0 & 0 \end{pmatrix}$

[a]Groups $4'mm'$ ($x_{1,2} \perp m$ planes) and $4'm'm$ ($x_{1,2} \perp m'$ planes) are equivalent within the rotation of the coordinate system.

pearance of PM effect was not proved theoretically.[19] The surface influence on ME properties was studied from the first principles for a few ferromagnetic materials only[20] while PM effects in nanosystems were not considered so far.

The above facts motivated us to use symmetry theory to explore how the surface induces PM, PE effects, and linear ME coupling in nanosystems. Below we will show that in small enough nanosystems with a large surface-to-volume ratio new phases and phenomena such as size-dependent PM, PE, and linear ME effects appear, though they are absent in the corresponding bulk materials. The reasons for the appearance of these phases are the built-in magnetic and electric fields originating from surface piezoeffects coupled with the surface stresses in nanospheres, nanowires, and nanotubes as well as mismatch strains in thin films on substrates.

II. SYMMETRY THEORY CONSIDERATIONS OF THE PE, PM, AND ME TENSORS

It should be stressed that these effects can appear in all 90 magnetic classes. In bulk materials the PM effect could exist in 66 magnetic classes.[21] The number is obtained as a difference between the total number of magnetic classes (90) and the number (21) of magnetic classes, which possess operations of time reversal and space inversion simultaneously, and three classes of cubic symmetry ($m3m$, $m'3m'$, and $m'3m$). It is obvious that because the inversion center is

absent in the vicinity of surface for nanomaterials of arbitrary geometry, the PM effect has to exist in the aforementioned 21 magnetic classes, too. Our calculations, presented below, have shown that the PM effect also appeared in the nanomaterials, whose bulk symmetry group belongs to the above-mentioned three cubic classes. Therefore, contrary to the bulk, in nanomaterials the PM effect has to exist in 90 bulk magnetic classes.

The PM tensor that couples the axial magnetic field vector **H** with the polar strain tensor u_{ij} is a third-rank axial tensor $d_{ijk}^{(m)}$. Because the components of any tensor are defined by its transformation laws, let us consider quantitatively the form of the piezomagnetic tensors present in nanomaterials. To find out the nonzero components of third-rank tensors we will use the system of linear equations obtained from the transformation laws for the axial ($d_{lpn}^{(m)}$) and polar ($d_{lmn}^{(e)}$) third-rank tensors describing PM (m) and PE (e) effects in bulk,[21]

$$\tilde{d}_{ijk}^{(m)} = (-1)^{tr} \det(\mathbf{A}) A_{il} A_{jp} A_{kn} d_{lpn}^{(m)}, \quad \tilde{d}_{ijk}^{(e)} = A_{il} A_{jm} A_{kn} d_{lmn}^{(e)}. \tag{1}$$

Here the summation is performed over the repeating indexes. **A** is the transformation matrix with components A_{ij} ($i,j = 1,2,3$) and determinant $\det(\mathbf{A}) = \pm 1$; the factor tr denotes either the presence ($tr=1$) or the absence ($tr=0$) of the time-reversal operation coupled to the space transformation A_{ij}. For the case when the matrices **A** represent all the generating

TABLE II. Surface built-in fields H^b, E^b, and ME coupling coefficients for different nanosystems.

	Thin film of thickness h on a rigid substrate, surface normal $\uparrow\uparrow x_3$	Wire of the radius R, wire axes $\uparrow\uparrow z$, local normal $\mathbf{e}_\rho$ (cylindrical coordinates $\{\rho,\varphi,z\}$)	Sphere of radius R, local normal $\mathbf{e}_r$ (spherical coordinates $\{\rho,\theta,\varphi\}$)
Magnetic field H^b	$H_3^b = \dfrac{2u_m(d_{311}^{(Sm)}+d_{322}^{(Sm)})}{\mu_0\mu h(s_{11}+s_{12})}$, u_m is misfit strain, s_{ij} are compliances	$H_\rho^b = -\dfrac{2\tau(d_{\rho\varphi\varphi}^{(Sm)}+d_{\rho\rho\rho}^{(Sm)})}{\mu_0\mu R^2}$, τ is the intrinsic surface stress tensor coefficient[a]	$H_r^b = -\dfrac{6\tau(d_{r\theta\theta}^{(Sm)}+d_{rrr}^{(Sm)}+d_{r\varphi\varphi}^{(Sm)})}{\mu_0\mu R^2}$, τ is the intrinsic surface stress tensor coefficient
Electric field E^b	$E_3^b = \dfrac{2u_m(d_{311}^{(Se)}+d_{322}^{(Se)})}{\varepsilon_0\varepsilon h(s_{11}+s_{12})}$	$E_\rho^b = -\dfrac{2\tau(d_{\rho\varphi\varphi}^{(Se)}+d_{\rho\rho\rho}^{(Se)})}{\varepsilon_0\varepsilon R^2}$	$E_r^b = -\dfrac{6\tau(d_{r\theta\theta}^{(Se)}+d_{rrr}^{(Se)}+d_{r\varphi\varphi}^{(Se)})}{\varepsilon_0\varepsilon R^2}$
ME coupling	$\gamma_{3j}^R = \gamma_{3j} + \dfrac{\gamma_{3j}^S}{h} + \dfrac{d_{3kl}^{(Se)}d_{jkl}^{(Sm)}}{h^2(s_{11}+s_{12})}$	$\gamma_{ij}^R = \gamma_{ij} + \dfrac{2}{R}\gamma_{ij}^S$	$\gamma_{ij}^R = \gamma_{ij} + \dfrac{3}{R}\gamma_{ij}^S$

[a]Reference 32.

elements of the material point symmetry group (considered hereinafter) the identity $\widetilde{d}_{ijk}^{(m,e)} \equiv d_{ijk}^{(m,e)}$ should be valid for nonzero components of the piezotensors.

For any spatially confined system the inversion center disappears in the surface-normal direction and only the symmetry axes and planes normal to the surface are conserved. Thus the magnetic and space symmetry group should be reduced to one of its subgroup, consisting of the transformation matrices A_{ij}^S, which satisfy the relations $n_i A_{ij}^S n_j = 1$, where n_j are the components of the surface normal. As a result the surface piezoeffect tensors $d_{lpn}^{(Sm)}$ and $d_{lmn}^{(Se)}$ (existing even in a cubic symmetry lattice near the surface) should obey other transformation laws than the ones existing in the bulk material, namely, $d_{ijk}^{(Sm)} \equiv (-1)^{tr}\det(\mathbf{A}^S) A_{il}^S A_{jp}^S A_{kn}^S d_{lpn}^{(Sm)}$ and $d_{ijk}^{(Se)} \equiv A_{il}^S A_{jm}^S A_{kn}^S d_{lmn}^{(Se)}$.

In the same way one can analyze the second-rank ME tensor γ_{ij}. The transformation laws for the linear surface ME axial tensor γ_{ij}^S are $\widetilde{\gamma}_{ij}^S = (-1)^{tr}\det(\mathbf{A}^S) A_{ik}^S A_{il}^S \gamma_{kl}^S$ and $\widetilde{\gamma}_{ij}^S \equiv \gamma_{ij}^S$ for nonzero components, i.e., the laws differ from the ones existing in the bulk material: $\widetilde{\gamma}_{ij} = (-1)^{tr}\det(\mathbf{A}) A_{ik} A_{il} \gamma_{kl}$. In the bulk the ME effect was shown to exist in 58 magnetic classes.[21] The analysis, similar to the one we performed for the piezomagnetic tensor, shows that the ME effect exists in nanosystems in 90 magnetic classes. Thus new piezomagnetics, piezoelectrics, and linear magnetoelectrics should appear even among nanomaterials, which are nonpiezomagnetic and nonpiezoelectric in the bulk but belong to the one of the existing 90 bulk magnetic classes, e.g., simple binary oxides such as EuO, CoO, and Er_2O_3. Note that similar arguments

could be applied to the different physical phenomena described by tensorial coupling between magnetic field and other physical fields. Thus, new terms in galvanic and thermomagnetic effects such as Hall, Righi-Leduc, Nernst-Ettingshausen, and magnetoresistance should appear for nanosystems of magnetic materials.

To demonstrate this intriguing possibility, we calculate the form of the surface PE, PM, and ME tensors for the bulk $m3m$, $m'3m'$, $m'3m$, and $m3m'$ cubic symmetry groups (symbol prime stands for the coupling with time reversal). The surface $4mm$, $4m'm'$, $4'm'm$, and $4'mm'$ symmetry groups were directly obtained from the bulk $m3m$, $m'3m'$, $m'3m$, and $m3m'$ symmetry groups, respectively, by considering the surface normal $x_3 \uparrow\uparrow 4$ (symbol 4 stands for the fourth-order rotation axis). Note, that the bulk symmetry groups correspond to the nonpiezoelectric binary oxides MnO, FeO, CoO, NiO, MnS, EuO, PrO, and Er_2O_3.

Results for $d_{ijk}^{(Sm)}$, $d_{ijk}^{(Se)}$, and γ_{ij}^S are presented in Table I. It is seen that all above-mentioned cubic materials become PE and PM in the vicinity of surface with different $d_{ijk}^{(Sm)}$ tensors, which depend on the surface symmetry group. The influence of the surface on the symmetry and properties is essential at distances of several tens of nanometers from the surface.[22,23] It is seen that the surface influences the number and type of nonzero components of PE, PM, and ME tensors.

Nonmagnetoelectric bulk materials of cubic symmetry become linear ME in the vicinity of surface with different γ_{ij}^S tensors, which depend on the surface symmetry group. ME bulk materials with $m'3m'$ symmetry remain linear ME in the vicinity of surface but the symmetry of γ_{ij}^S changes in

TABLE III. Material parameters of typical binary oxide used in calculations.

|		
Surface ME, PE, and PM tensors	$\gamma_{ij}^S = 2\times10^{-11}\times a\times\text{s/m}$; where the lattice constant $a = (0.4-0.5)\times10^{-9}$ m; $d_{31}^{Se} = -1.63\times10^{-11}\times a\times\text{m/V}$, $d_{33}^{Se} = 3.82\times10^{-11}\times a\times\text{m/V}$, $d_{15}^{Se} = -0.86\times10^{-11}\times a\times\text{m/V}$; $d_{31}^{Sm} = -1.0\times10^{-9}\times a\times\text{m/A}$, $d_{33}^{Sm} = 3.0\times10^{-9}\times a\times\text{m/A}$, $d_{15}^{Sm} = -0.5\times10^{-9}\times a\times\text{m/A}$	21 and 38
Elastic modules	$s_{11} = 10.23\times10^{-12}$ Pa^{-1}, $s_{12} = -2.91\times10^{-12}$ Pa^{-1}, $s_{44} = 29.67\times10^{-12}$ Pa^{-1}; $c_{11} = 126.1\times10^9$ Pa, $c_{12} = 50.0\times10^9$ Pa, $c_{44} = 33.7\times10^9$ Pa	38
Others	$\varepsilon_0 = 8.85\times10^{-12}$ F/m, $\mu_0 = 4\pi\times10^{-7}$ N/A^2, relative permittivities $\varepsilon = 30$, $\mu = 1$, surface stress coefficient $\tau = 10$ N/m, mismatch strain $u_m = (2-4)\times10^{-3}$	38 and 39
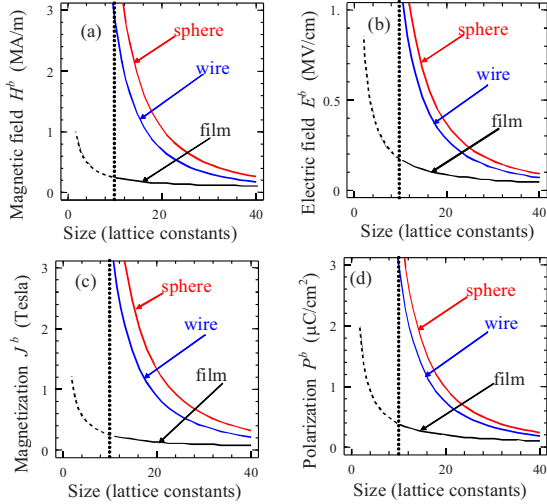
FIG. 1. (Color online) Dependences of the built-in (a) magnetic and (b) electric fields, (c) surface-induced magnetization and (d) polarization on system size in the lattice constant units (film thickness h/a, wire, or spherical particle diameter $2R/a$). Our continuous media model can be quantitatively valid in the region right to the vertical dotted lines.

comparison with the bulk tensor γ_{ij} (see the last row in Table I).

Thus symmetry breaking inevitably present in the vicinity of the any surface gives rise to new PM, PE, and ME effects in nanosystems while these effects can be absent in a bulk material. The linear ME effect can exist in nanosystems made of materials belonging to the all 90 bulk magnetic classes. So the number of ME classes in nanomaterials is much larger than in the bulk (58). The proposed method for the evaluation of the nonzero components of PM, PE, and ME tensors for nanomaterials of different geometry was applied to all 90 bulk magnetic groups and the obtained results will be published elsewhere.

Below we demonstrate that the surface piezomagnetic and piezoelectric effects coupled with the surface stress for nanoparticles and mismatch strains for thin films on substrates lead to the appearance of built-in magnetic and electric fields. These fields lead to appearance of magnetization or polarization and so to the change in phase diagrams.

III. SIZE EFFECTS OF THE PE, PM, AND ME TENSORS INHERENT TO NANOSYSTEMS

To consider the size effects of a confined system let us represent the free energy as $G = \int_S g_S d^2 r + \int_V g_V d^3 r$. The surface energy contribution increases with the decrease in the system's size, i.e., it increases with increasing (S/V) ratio (here S is the system surface and V is its volume). In the adopted model the part of the free energy we are interested in, namely, the one dependent on piezocoupling and ME coupling of electric (E_i) and magnetic (H_i) fields, can be written as

$$\Delta G_R = -(d_{ijk}^{(e)}\sigma_{jk}E_i + d_{ijk}^{(m)}\sigma_{jk}H_i + \varepsilon_0\varepsilon E_i^b E_i + \mu_0\mu H_i^b H_i + \gamma_{ij}^R H_i E_j)V. \qquad (2)$$

The energy includes the built-in magnetic H_i^b

$= d_{ijk}^{(Sm)}\sigma_{jk}S/\mu_0\mu V$, electric $E_i^b = d_{ijk}^{(Se)}\sigma_{jk}S/\varepsilon_0\varepsilon V$ fields (ε_0 and μ_0 are universal dielectric and magnetic constants, respectively, σ_{ij} is the stress tensor) and magnetoelectric energy density $\gamma_{ij}^R H_i E_j$ with renormalized ME coefficient $\gamma_{ij}^R \cong \gamma_{ij} + \gamma_{ij}^S S/V$, where γ_{ij}^S is listed in Table I.

The application of the continuum approach to the description of nanosystems properties needs some justification. The continuum approach was accepted for the analysis of the elastic properties of metallic, semiconductor, dielectric, or polymeric nanowires and nanotubes[24–27] and the piezoelectric response.[28] For nanosized ferroics the applicability of the continuous theory is corroborated by the fact that the critical sizes (~ 2–10 lattice constants) of the appearance of long-range order calculated from atomistic[29] and phenomenological theories[19] are in a good agreement with each other[30,31] as well as with experimental results.[8,12]

It is seen from Table II, that the built-in fields H_i^b and E_i^b and the linear ME coupling γ_{ij}^R (produced by the surface $4mm$, $4m'm'$, $4'mm'$, and $4'm'm$ symmetry groups) spontaneously arise for the typical cases of ultrathin films, nano-
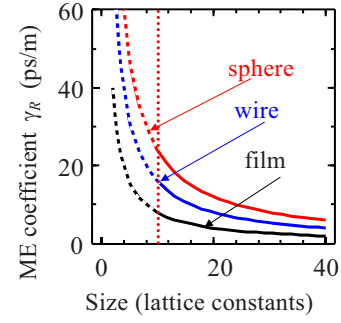

FIG. 2. (Color online) Dependences of the linear ME coefficient on the nanosystem characteristic size (film thickness h/a, wire, or spherical particle diameter $2R/a$). The linear ME coupling is regarded absent in the bulk material.
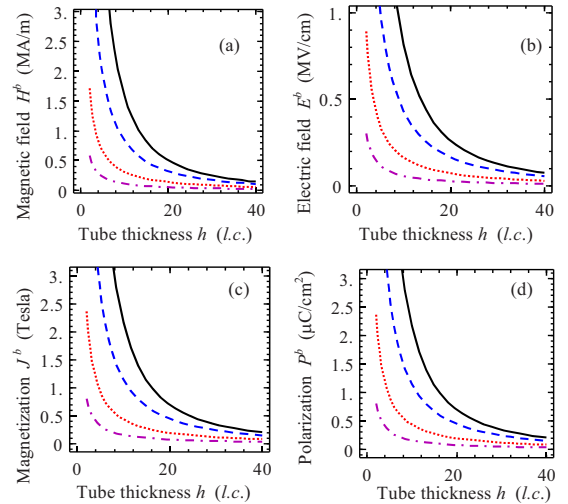

FIG. 3. (Color online) Dependences of the built-in (a) magnetic and (b) electric fields, (c) surface-induced magnetization and (d) polarization on the on the tube thickness $h = R - r$ (in lattice constants) at the fixed inner radius $r = 2, 6, 20, 60$ l.c. (solid, dashed, dotted, and dashed-dotted curves).

wires, nanotubes, and nanospheres. So, a large number of new linear magnetoelectrics should appear among nanosystems, which are nonmagnetoelectric in the bulk. It is necessary to underline that the values of the built-in fields and ME coupling increase with the decrease in film thickness h or nanoparticles radii R. The obtained analytical dependencies for thin films or nanoparticles, respectively, have shown that H_i^b and $E_i^b \sim 1/h$ or $1/R^2$ while the ME coupling γ_{ij}^R is inversely proportional to the sizes in both cases. This shows the strong influence of sizes on the properties of nanomaterials.

Expressions for the stress tensor σ_{ij} were obtained from the mechanical problem solutions with appropriate boundary conditions, which are summarized in Table IV of Appendix (see also Ref. 33). Note, that the fields and ME coupling coefficient breakdown related to the divergences such as $1/\text{size}$ or $1/\text{size}^2$ is not achieved, since the continuous model can be quantitatively valid until the system's actual size is substantially larger than the lattice constant a (e.g., for film thicknesses $h > 10a$ and particle diameters $2R > 10a$ larger than several lattice constant).

Let us underline that we considered an ideal surfaces, free of the relaxations, rumplings, and reconstructions. Such "atomically sharp" surfaces and interfaces become reality for the current state of art in nanotechnology (see, e.g., Refs. 34 and 35). On the other hand sometimes the surface reconstruction gives rise to the surface tension, necessary for the observation of built-in fields predicted by us in the nanoparticles. Actually, Zang et al.[36,37] have found that the surface reconstruction is responsible for the appearance of surface stresses and leads to the self-bending of Si nanofilms. This effect depends on the adsorption characteristics.[37] Since the surface tension appears even for the case of nonreconstructed geometrical surface due to the surface break,[32] the surface transformation could, in principle, affect the surface tension value.

Below we compare our analytical results with the typical experimental values of magnetic anisotropy field, coercive fields, spontaneous magnetization, and polarization found in the literature, and obtained that they are relatively high.

Dependences of the built-in magnetic $H_\rho^b \cong d_{\rho jk}^{(Sm)} \sigma_{jk} S / \mu \mu_0 V$ and electric $E_\rho^b \cong d_{\rho jk}^{(Se)} \sigma_{jk} S / \varepsilon \varepsilon_0 V$ fields, surface-induced magnetization $J_\rho^b \cong d_{\rho jk}^{(Sm)} \sigma_{jk} S / V$, and polarization $P_\rho^b \cong d_{\rho jk}^{(Se)} \sigma_{jk} S / V$ on the system size were calculated using analytical expressions from Table I and are shown in Fig. 1. The size dependence of the surface-induced ME coefficient is shown in Fig. 2.

Dependences of the built-in magnetic and electric fields, surface-induced magnetization, and polarization on the thickness h of the free-standing tube are shown in Fig. 3. It is seen that the built-in magnetic and electric fields, magnetization, and polarization monotonically increase as $1/h$ with the tube thickness decrease. The decrease in the tube inner radius increases the values of built-in fields, polarization, and magnetization (compare different curves plotted for different r).

It is seen from the Figs. 1–3 that the built-in magnetic and electric fields, induced magnetization, polarization, and ME coefficient values monotonically increase as $1/\text{size}$ with the size decrease. Also they are maximal for spheres, intermediate for tubes or wires, and minimal for films at the same h

value. The result is expected from the difference of geometrical ratio S/V that is equal to $3/h$ for spheres, $2/h$ for tubes or wires, and $1/h$ for thin films. It is seen from the Figs. 1–3 that predicted PM, PE, and ME effects can be significantly enhanced (in orders of magnitude) in nanosized particles and thin films by choosing appropriate sizes.

Typical values of magnetic anisotropy field (H_a) and spontaneous magnetization J_S listed in literature are within the range $H_a \sim 0.1$–1 MA/m and $J_S = 0.5$–2 T. Typical values of coercive electric field E_c and spontaneous polarization P_S listed in literature vary in the range $E_c = 0.1$–1 MV/cm and $P_S \sim 0.5$–100 $\mu C/cm^2$. Figures 1 and 3 show that relatively high values $H_b \sim 0.5$–2 MA/m, $J_b \sim 0.2$–2 T, $E_b \sim 0.1$–1 MV/cm, and moderate polarization $P_S \sim 0.5$–2 $\mu C/cm^2$ are achievable for nanosystems with sizes below 20–10 l.c. (i.e., about 10–5 nm). The calculated fields values are rather underestimated than overestimated since for the estimations of the surface PE (d_{ij}^{Se}) and PM (d_{ij}^{Sm}) tensor components we used typical bulk values of the bulk PE and PM tensor components multiplied on the lattice constant a (Table III).

Note, that ME coefficient values listed in literature is about 30 pm/s.[13] Figure 2 shows that such values as 5–20 pm/s are achievable for ultrathin films and nanoparticles due to the strong size effects at sizes below 20–10 l.c., which is about 10–5 nm. The calculated values are rather underestimated than overestimated since we used typical bulk amplitude $\sim 10^{-11}$ s/m multiplied on the lattice constant $a \sim 0.5$ nm for the estimations of the surface ME tensor γ_{ij}^S (Table III). Keeping in mind that electro-optical effect and nonlinear susceptibilities are defined by third-rank tensors, the results presented in the second and third columns of Table I can be applied for these effects also.

Since all our predictions are based on the symmetry theory only, but not on the first principles atomistic calculations, we should underline that although the surface-induced symmetry lowering (usually connected with the reduction in coordination number) proclaims the possibility of the magnetic moments appearance at the surface, the microscopic physical mechanisms, which lead to the magnetism origin and determine its peculiarities should be manifold and thus a separate first-principles based study is required in every concrete case. For instance, nonmagnetic vanadium can be magnetic in ultrathin film configuration; but the magnetic moments originate due to reduced coordination in vanadium monolayers, rather than symmetry lowering.[40] The effect of reduced coordination leads to the antiferromagnetic properties of the monolayer iron placed on the W(001) substrate.[41]
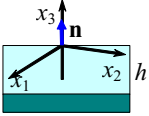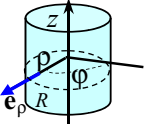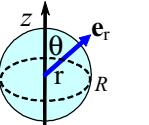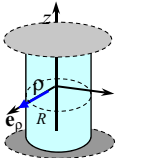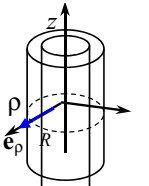
IV. SUMMARY

Piezomagnetic, piezoelectric effects, and size-dependent linear magnetoelectric coupling are predicted in nanosystems, which are nonpiezomagnetic and nonpiezoelectric in the bulk, but correspond to one of the 90 magnetic classes. Coupled with a surface stress in nanoparticles and strains in thin films, the piezoeffects lead to the appearance of size-dependent magnetic and electric built-in fields, which in turn can induce self-polarization and self-magnetization of nano-

sized oxides such as MnO, FeO, CoO, NiO, MnS, EuO, PrO, and Er_2O_3. The symmetry breaking inevitably present the vicinity of the nanosystem surface could lead to novel linear electro-optical and magneto-optical coupling as well as new terms in the nonlinear susceptibilities. New terms in galvanic and thermomagnetic effects such as Hall, Righi-Leduc,

Nernst-Ettingshausen, and magnetoresistance should appear for thin films and small enough nanoparticles; corresponding tensors could be calculated by in same way we proposed here for the surface piezomagnetic and magnetoelectric tensors. These theoretical forecasts should stimulate experimental investigation.

APPENDIX

TABLE IV. (Color online) Stress components and built-in fields in nanosystems of different geometry.

Nanosystem	Boundary conditions	Stress components and built-in fields
Thin film of thickness h on a rigid substrate, surface normal $\uparrow\uparrow x_3$	$\sigma_{3i}\|_{z=0}=0$ $u_{11}=u_{22}\|_{z=h}=u_m,$ $i=1,2,3,$ u_m is misfit strain	Stresses in Cartesian coordinates: $\sigma_{11}=\frac{u_m}{s_{11}+s_{12}}-\frac{E_i(s_{11}d_{i11}^{(Se)}-s_{12}d_{i22}^{(Se)})-H_i(s_{11}d_{i11}^{(Sm)}-s_{12}d_{i22}^{(Sm)})}{h(s_{11}^2-s_{12}^2)},$ $\sigma_{22}=\frac{u_m}{s_{11}+s_{12}}-\frac{E_i(s_{11}d_{i22}^{(Se)}-s_{12}d_{i11}^{(Se)})-H_i(s_{11}d_{i22}^{(Sm)}-s_{12}d_{i11}^{(Sm)})}{h(s_{11}^2-s_{12}^2)},$ $\sigma_{31}=\sigma_{32}=\sigma_{33}=0$ Built-in fields: $H_3^b=\frac{2u_m(d_{311}^{(Sm)}+d_{322}^{(Sm)})}{\mu_0\mu h(s_{11}+s_{12})},\qquad E_3^b=\frac{2u_m(d_{311}^{(Se)}+d_{322}^{(Se)})}{\varepsilon_0\varepsilon h(s_{11}+s_{12})}$
Wire of the radius R, wire axes $\uparrow\uparrow z$, local normal $\mathbf{e}_\rho$	$\sigma_{\rho\rho}\|_{\rho=R}=-\frac{\tau}{R},$ $\sigma_{\rho z}=\sigma_{\rho\varphi}\|_{\rho=R}=0,$ $\sigma_{z\rho}=\sigma_{z\varphi}=\sigma_{zz}\|_{z=\pm h/2}=0$	Stresses in cylindrical coordinates $\{\rho,\varphi,z\}$: $\sigma_{\rho\rho}=\sigma_{\varphi\varphi}=-\frac{\tau}{R},\quad \sigma_{\rho\varphi}=\sigma_{\rho z}=\sigma_{zz}=\sigma_{z\varphi}=0,$ τ is the intrinsic surface stress tensor coefficient Built-in fields: $H_\rho^b=-\frac{2\tau(d_{\rho\varphi\varphi}^{(Sm)}+d_{\rho\rho\rho}^{(Sm)})}{\mu_0\mu R^2},\qquad E_\rho^b=-\frac{2\tau(d_{\rho\varphi\varphi}^{(Se)}+d_{\rho\rho\rho}^{(Se)})}{\varepsilon_0\varepsilon R^2}$
Nanosphere of radius R, local normal is $\mathbf{e}_r$	$\sigma_{rr}\|_{r=R}=-\frac{2\tau}{R},$ $\sigma_{r\varphi}\|_{r=R}=\sigma_{r\theta}\|_{r=R}=0$	Stresses in spherical coordinates $\{r,\theta,\varphi\}$: $\sigma_{rr}=\sigma_{\theta\theta}=\sigma_{\varphi\varphi}=-\frac{2\tau}{R},\quad \sigma_{r\theta}=\sigma_{r\varphi}=0$ Built-in fields: $H_r^b=-\frac{6\tau(d_{r\theta\theta}^{(Sm)}+d_{rrr}^{(Sm)}+d_{r\varphi\varphi}^{(Sm)})}{\mu_0\mu R^2},$ $E_r^b=-\frac{6\tau(d_{r\theta\theta}^{(Se)}+d_{rrr}^{(Se)}+d_{r\varphi\varphi}^{(Se)})}{\varepsilon_0\varepsilon R^2}$
Clamped nanowire of radius R, wire axes $\uparrow\uparrow z$, local normal $\mathbf{e}_\rho$	$\sigma_{\rho\rho}\|_{\rho=R}=-\frac{\tau}{R},$ $\sigma_{\rho z}=\sigma_{\rho\varphi}\|_{\rho=R}=0,$ $\sigma_{z\rho}=\sigma_{z\varphi}\|_{z=\pm h/2}=0,$ $u_z\|_{z=\pm h/2}=0$	Stresses and strains in cylindrical coordinates $\{\rho,\varphi,z\}$: $\sigma_{\rho\rho}=\sigma_{\varphi\varphi}=-\frac{\tau}{R},\quad \sigma_{zz}=\frac{s_{12}}{s_{11}}\frac{2\tau}{R},$ $\sigma_{\rho\varphi}=\sigma_{\rho z}=\sigma_{z\varphi}=0,$ τ is the intrinsic surface stress tensor coefficient Built-in fields: $H_\rho^b=-\frac{2\tau}{\mu_0\mu R^2}\left(d_{\varphi\varphi\varphi}^{(Sm)}+d_{\rho\rho\rho}^{(Sm)}-2d_{\rho zz}^{(Sm)}\frac{s_{12}}{s_{11}}\right),$ $E_\rho^b=-\frac{2\tau}{\varepsilon\varepsilon_0 R^2}\left(d_{\varphi\varphi\varphi}^{(Se)}+d_{\rho\rho\rho}^{(Se)}-2d_{\rho zz}^{(Se)}\frac{s_{12}}{s_{11}}\right)$
Free-standing nanotube with outer radius R, inner radius r	$\sigma_{\rho\rho}\|_{\rho=r}=+\frac{\tau}{R},$ $\sigma_{\rho\rho}\|_{\rho=R}=-\frac{\tau}{R},$ $\sigma_{\rho z}=\sigma_{\rho\varphi}\|_{\rho=r,R}=0,$ $\sigma_{z\rho}=\sigma_{z\varphi}=\sigma_{zz}\|_{z=\pm h/2}=0.$ The radial boundary conditions correspond to the surface bond elongation and contraction, respectively	$\sigma_{\rho\rho}+\sigma_{\varphi\varphi}=\sigma_{11}+\sigma_{22}=-\frac{\tau}{R+r},$ $\sigma_{\rho\varphi}=\sigma_{\rho z}=\sigma_{zz}=\sigma_{z\varphi}=0$ Built-in fields: $H_\rho^b=\frac{-4\tau d_{\rho\rho\rho}^{(Sm)}}{\mu\mu_0(R^2-r^2)}=\frac{-4\tau d_{\rho\rho\rho}^{(Sm)}}{\mu\mu_0 h(R+r)},$ $E_\rho^b=\frac{-4\tau d_{\rho\rho\rho}^{(Se)}}{\varepsilon\varepsilon_0(R^2-r^2)}=\frac{-4\tau d_{\rho\rho\rho}^{(Se)}}{\varepsilon\varepsilon_0 h(R+r)}.$ Tube thickness is $h=R-r$. $\gamma_{ij}^R=\gamma_{ij}+\frac{2}{h}\gamma_{ij}^S.$ The expressions are derived for the case $d_{\rho\varphi\varphi}^{(Sm)}=d_{\rho\rho\rho}^{(Sm)}$

*Corresponding author; eliseev@i.com.ua

[1] M. Bode, M. Heide, K. von Bergmann, P. Ferriani, S. Heinze, G. Bihlmayer, A. Kubetzka, O. Pietzsch, S. Blügel, and R. Wiesendanger, Nature (London) **447**, 190 (2007).

[2] H. De Raedt, S. Miyashita, K. Michielsen, and M. Machida, Phys. Rev. B **70**, 064401 (2004).

[3] M. Heide, G. Bihlmayer, and S. Blügel, Phys. Rev. B **78**, 140403(R) (2008).

[4] A. N. Rudenko, V. V. Mazurenko, V. I. Anisimov, and A. I. Lichtenstein, Phys. Rev. B **79**, 144418 (2009).

[5] A. Sundaresan, R. Bhargavi, N. Rangarajan, U. Siddesh, and C. N. R. Rao, Phys. Rev. B **74**, 161306(R) (2006).

[6] Y. Nakae, Y. Seino, T. Teranishi, M. Miyake, S. Yamada, and H. Hori, Physica B **284-288**, 1758 (2000).

[7] P. Ayyub, S. Chattopadhyay, R. Pinto, and M. S. Multani, Phys. Rev. B **57**, R5559 (1998).

[8] D. Yadlovker and S. Berger, Phys. Rev. B **71**, 184112 (2005).

[9] J. H. Haeni, P. Irvin, W. Chang, R. Uecker, P. Reiche, Y. L. Li, S. Choudhury, W. Tian, M. E. Hawley, B. Craigo, A. K. Tagantsev, X. Q. Pan, S. K. Streiffer, L. Q. Chen, S. W. Kirchoefer, J. Levy, and D. G. Schlom, Nature (London) **430**, 758 (2004).

[10] J. Wang, J. B. Neaton, H. Zheng, V. Nagarajan, S. B. Ogale, B. Liu, D. Viehland, V. Vaithyanathan, D. G. Schlom, U. V. Waghmare, N. A. Spaldin, K. M. Rabe, M. Wuttig, and R. Ramesh, Science **299**, 1719 (2003).

[11] A. N. Morozovska, M. D. Glinchuk, and E. A. Eliseev, Phys. Rev. B **76**, 014102 (2007).

[12] Sudip Mukherjee, Ching Hsuan Chen, Chih Chieh Chou, Bijay Krishna Chaudhuri, and Hung-Duen Yang, APS March Meeting, 15–19 March, 2010 (unpublished).

[13] M. Fiebig, J. Phys. D: Appl. Phys. **38**, R123 (2005).

[14] W. Eerenstein, N. D. Mathur, and J. F. Scott, Nature (London) **442**, 759 (2006).

[15] J. F. Scott, Nature Mater. **6**, 256 (2007).

[16] V. M. Petrov, G. Srinivasan, M. I. Bichurin, and A. Gupta, Phys. Rev. B **75**, 224407 (2007).

[17] E. Roduner, *Nanoscopic Materials: Size-Dependent Phenomena* (RSC, Cambridge, United Kingdom, 2006).

[18] M. D. Glinchuk and A. N. Morozovska, J. Phys.: Condens. Matter **16**, 3517 (2004).

[19] M. D. Glinchuk, E. A. Eliseev, A. N. Morozovska, and R. Blinc, Phys. Rev. B **77**, 024106 (2008).

[20] C.-G. Duan, J. P. Velev, R. F. Sabirianov, Z. Zhu, J. Chu, S. S. Jaswal, and E. Y. Tsymbal, Phys. Rev. Lett. **101**, 137201 (2008).

[21] *Modern Crystallography, Vol. IV: Physical Properties of Crystals*, Springer Series in Solid-State Sciences, edited by L. A. Shuvalov (Springer-Verlag, Berlin, 1988).

[22] M. F. Deigen and M. D. Glinchuk, Surf. Sci. **3**, 243 (1965).

[23] C.-L. Jia, V. Nagarajan, J.-Q. He, L. Houben, T. Zhao, R. Ramesh, K. Urban, and R. Waser, Nature Mater. **6**, 64 (2007).

[24] S. Cuenot, C. Frétigny, S. Demoustier-Champagne, and B. Nysten, Phys. Rev. B **69**, 165410 (2004).

[25] G. Y. Jing, H. L. Duan, X. M. Sun, Z. S. Zhang, J. Xu, Y. D. Li, J. X. Wang, and D. P. Yu, Phys. Rev. B **73**, 235409 (2006).

[26] G. Stan, C. V. Ciobanu, P. M. Parthangal, and R. F. Cook, Nano Lett. **7**, 3691 (2007).

[27] E. Hernández, C. Goze, P. Bernier, and A. Rubio, Phys. Rev. Lett. **80**, 4502 (1998).

[28] Yifan Gao and Zhong Lin Wang, Nano Lett. **7**, 2499 (2007).

[29] J. Hong, G. Catalan, D. N. Fang, E. Artacho, and J. F. Scott, Phys. Rev. B **81**, 172101 (2010).

[30] M. Q. Cai, Y. Zheng, B. Wang, and G. W. Yang, Appl. Phys. Lett. **95**, 232901 (2009).

[31] M. S. Majdoub, R. Maranganti, and P. Sharma, Phys. Rev. B **79**, 115412 (2009).

[32] V. A. Shchukin and D. Bimberg, Rev. Mod. Phys. **71**, 1125 (1999).

[33] E. A. Eliseev, A. N. Morozovska, M. D. Glinchuk, B. Y. Zaulychny, V. V. Skorokhod, and R. Blinc, arXiv:0912.5010 (unpublished).

[34] Ming-Wen Chu, Izabela Szafraniak, Roland Scholz, Catalin Harnagea, Dietrich Hesse, Marin Alexe, and Ulrich Gösele, Nature Mater. **3**, 87 (2004).

[35] J. C. Jiang, X. Q. Pan, W. Tian, C. D. Theis, and D. G. Schlom, Appl. Phys. Lett. **74**, 2851 (1999).

[36] J. Zang, M. Huang, and F. Liu, Phys. Rev. Lett. **98**, 146102 (2007).

[37] J. Zang and F. Liu, Nanotechnology **18**, 405501 (2007).

[38] O. Madelung, *Semiconductors: Data Handbook*, 3rd ed. (Springer Verlag, Berlin, 2004).

[39] W. Ma, M. Zhang, and Z. Lu, Phys. Status Solidi A **166**, 811 (1998) a.

[40] S. Blügel, Phys. Rev. Lett. **68**, 851 (1992).

[41] A. Kubetzka, P. Ferriani, M. Bode, S. Heinze, G. Bihlmayer, K. von Bergmann, O. Pietzsch, S. Blügel, and R. Wiesendanger, Phys. Rev. Lett. **94**, 087204 (2005).